URSI GASS 2021, Rome, Italy, 28 August - 4 September 2021

Designing Metasurfaces to Manipulate Antenna Radiation

J. R. Capers[(1)], S. J. Boyes[(2)], A. P. Hibbins[(1)] and S. A. R. Horsley[(1)]
(1) Electromagnetic and Acoustic Materials Group, Department of Physics and Astronomy,
University of Exeter, Stocker Road, EX4 4QL
(2) DSTL Porton Down, Salisbury, Wiltshire, SP4 0JQ

Abstract

We derive a simple and efficient method for designing wave–shaping materials composed of dipole scatterers, taking into account multiple scattering effects and both magnetic and electric polarizabilities. As an application of our theory, we design a-periodic metasurfaces that re-structure the radiation from a dipole emitter: (i) modifying of the near-field to provide a 3 fold enhancement in power emission; (ii) re-shaping the far-field radiation pattern to exhibit chosen directivity; and (iii) the design of a discrete 'Luneburg lens'. Our proposed technique is relevant to designing metamaterials for a wide class of applications, and has the key benefit of including all interactions within the system of scatterers. Additionally, we develop a clear physical interpretation of the optimized structure, by extracting 'eigenpolarizabilities' of the system, finding that a large 'eigenpolarizability' corresponds to a large collective response of the scatterers.

1 Introduction

Designing the scattering properties of materials is a fundamental challenge in a broad range of disciplines, from metamaterial design [1] to imaging through disordered media [2]. In recent years, there has been increasing interest in how appropriately designed metamaterials can induce virtually any desired wave effect, be that acoustic [3] or electromagnetic [4]. To solve this problem the connection between incident and scattered fields must be established, and then this must be used to design the metamaterial structure.

Recent interesting developments include 'metalenses', which can have superior bandwidth to traditional refractive lenses [5], as well as metasurface antennas [6]. Metasurface antennas present the opportunity to engineer bespoke beam-shaping, steering, polarization control and improve efficiency [6]. Several classes of metasurface have been designed using an algorithm to selectively place scattering elements to form a metasurface with specific properties. This principle has been used to design metasurface holograms [7], and for wavefront shaping [8]. What unites the seemingly disparate applications of holograms, metalenses and wavefront shaping is the problem of designing materials to realise a given wave effect.

The materials required for each of these functionalities can be designed using very similar methods. For example, holograms [7], metalenses [5] and beam shaping surfaces [6] have all been designed using the Gercherg-Saxton algorithm. However, this method neglects multiple scattering interactions and assumes that only a local phase offset is imparted upon the incident field. This inhibits the application of this design method to problems were non-local interactions are key, for example in achieving perfect anomalous reflection [9].

Due to broad demand for methods to design the scattering properties of materials, the problem of devising design methodologies has attracted recent attention [10]. As well as the Gerchberg-Saxton, there are two other popular inverse design paradigms. Firstly, geometry optimisation based upon the adjoint design method has been used to design many electromagnetic structures [10]. Typically this procedure involves evaluating a cost function, which is to be extremised, over a given geometry using a full-wave solver. Changes to the geometry are then made iteratively, so that the figure of merit is improved until a convergence is reached. A key feature of the adjoint method is that the cost function contains both a 'forward' and an 'inverse' contribution. Reciprocity is exploited to allow the 'forward' and 'inverse' parts to be calculated together, reducing the number of numerical simulations required to determine how material parameters should be changed. Secondly, machine learning [11] and genetic algorithms [12] have become extremely popular for solving the inverse design problem due to their ability to traverse large search spaces. While machine learning has a role to play in optimisation processes, applying analytic techniques to the problem can provide more time-efficient design. It is the ambition of our current work to seek a design method that admits a clear physical interpretations of both the optimisation method and of the results, while being numerically efficient.

In this work we present two contributions. Leveraging the benefits of adjoint algorithms, we propose a semi-analytic framework to design the scattering properties of non-periodic arrangements of discrete dipolar scatterers. We account for all interactions so that all multiple-scattering effects are considered. By examining these strongly non-local properties of the entire scattering system, we suggest

an interpretation of the eigenvalues of the scattering system. This provides explanatory detail on the mechanisms behind the optimisation procedure. Together, these techniques provide a new paradigm for the inverse design of metamaterials comprised of scatterers which are sub-wavelength but strongly coupled.

2 Designing Scattering Properties

For a system of N spherical, isotropic scatterers characterized by their electric and magnetic polarizability tensor, $\overleftrightarrow{\boldsymbol{\alpha}}_E$ and $\overleftrightarrow{\boldsymbol{\alpha}}_H$ respectively, the solutions to Maxwell's equations can be written as

$$\begin{pmatrix}\boldsymbol{E}(\boldsymbol{r})\\ \boldsymbol{H}(\boldsymbol{r})\end{pmatrix} = \begin{pmatrix}\boldsymbol{E}_s(\boldsymbol{r})\\ \boldsymbol{H}_s(\boldsymbol{r})\end{pmatrix} + \sum_{n=1}^{N}\begin{pmatrix}\xi^2\overleftrightarrow{\boldsymbol{G}}(\boldsymbol{r},\boldsymbol{r}_n)\overleftrightarrow{\boldsymbol{\alpha}}_E & i\xi\overleftrightarrow{\boldsymbol{G}}_{EH}(\boldsymbol{r},\boldsymbol{r}_n)\overleftrightarrow{\boldsymbol{\alpha}}_H\\ -i\xi\overleftrightarrow{\boldsymbol{G}}_{EH}(\boldsymbol{r},\boldsymbol{r}_n)\overleftrightarrow{\boldsymbol{\alpha}}_E & \xi^2\overleftrightarrow{\boldsymbol{G}}(\boldsymbol{r},\boldsymbol{r}_n)\overleftrightarrow{\boldsymbol{\alpha}}_H\end{pmatrix}\begin{pmatrix}\boldsymbol{E}(\boldsymbol{r}_n)\\ \boldsymbol{H}(\boldsymbol{r}_n)\end{pmatrix}, \tag{1}$$

where $(\boldsymbol{E}_s,\boldsymbol{H}_s)$ are the fields generated by a dipole source, ξ is a unitless wavenumber, $\overleftrightarrow{\boldsymbol{G}}(\boldsymbol{r},\boldsymbol{r'})$ is the electromagnetic Green's function and $\overleftrightarrow{\boldsymbol{G}}_{EH}(\boldsymbol{r},\boldsymbol{r'}) = \boldsymbol{\nabla}\times\overleftrightarrow{\boldsymbol{G}}(\boldsymbol{r},\boldsymbol{r'})$. The fields applied to each scatterer, $(\boldsymbol{E}(\boldsymbol{r}_n),\boldsymbol{H}(\boldsymbol{r}_n))$ include the field from the source as well as the field scattered by all other scatterers. The applied fields are determined by requiring self-consistency of the solution, which may be written as a matrix equation

$$\begin{pmatrix}\boldsymbol{E}(\boldsymbol{r}_1)\\ \boldsymbol{H}(\boldsymbol{r}_1)\\ \boldsymbol{E}(\boldsymbol{r}_2)\\ \boldsymbol{H}(\boldsymbol{r}_2)\\ \vdots\end{pmatrix} = \begin{pmatrix}\boldsymbol{R}_{11} & \boldsymbol{R}_{12} & \cdots\\ \boldsymbol{R}_{21} & \boldsymbol{R}_{22} & \cdots\\ \vdots & \vdots & \ddots\end{pmatrix}^{-1}\begin{pmatrix}\boldsymbol{E}_s(\boldsymbol{r}_1)\\ \boldsymbol{H}_s(\boldsymbol{r}_1)\\ \boldsymbol{E}_s(\boldsymbol{r}_2)\\ \boldsymbol{H}_s(\boldsymbol{r}_2)\\ \vdots\end{pmatrix}, \tag{2}$$

where $\boldsymbol{R}$ is the interaction matrix, defined as

$$\boldsymbol{R}_{ij} = \begin{pmatrix}\overleftrightarrow{\boldsymbol{I}}\delta_{ij} - \xi^2\overleftrightarrow{\boldsymbol{\alpha}}_E\overleftrightarrow{\boldsymbol{G}}(\boldsymbol{r}_i,\boldsymbol{r}_j) & -i\xi\overleftrightarrow{\boldsymbol{\alpha}}_H\overleftrightarrow{\boldsymbol{G}}_{EH}(\boldsymbol{r}_i,\boldsymbol{r}_j)\\ i\xi\overleftrightarrow{\boldsymbol{\alpha}}_E\overleftrightarrow{\boldsymbol{G}}_{EH}(\boldsymbol{r}_i,\boldsymbol{r}_j) & \overleftrightarrow{\boldsymbol{I}}\delta_{ij} - \xi^2\overleftrightarrow{\boldsymbol{\alpha}}_H\overleftrightarrow{\boldsymbol{G}}(\boldsymbol{r}_i,\boldsymbol{r}_j)\end{pmatrix}. \tag{3}$$

Eigenvalues of the interaction matrix can be viewed as 'eigen-polarizabilities' of the system. These can be interpreted as characterising the collective response of the scattering system. The effect of the photonic environment upon an emitter can be characterized using the Polarized (or Partial) Local Density of Optical States (PLDoS), defined as

$$\rho(\hat{\boldsymbol{p}},\boldsymbol{r},\omega) = \frac{2\varepsilon_0 n^2}{\pi\omega}\mathrm{Im}[\hat{\boldsymbol{p}}\cdot\boldsymbol{E}(\boldsymbol{r})]. \tag{4}$$

This gives the number of electromagnetic modes available per unit volume for a given source polarization, $\hat{\boldsymbol{p}}$, position $\boldsymbol{r}$ and frequency ω. It can be shown that the power emission of a dipole emitter is proportional to the PLDoS. The PLDoS provides a way to convert the properties of the scattering structure (with many free parameters) to a single positive real number. Due to this property, the PLDoS forms our figure of merit for the optimization procedure.

To design the scattering properties of the system of scatterers, we expand the solutions (1) in terms of small perturbations to the locations of the scatterers

$$\boldsymbol{r}_n \to \boldsymbol{r}_n + \Delta\boldsymbol{r}_n, \quad \boldsymbol{E} \to \boldsymbol{E}_0 + \boldsymbol{E}_1, \quad \boldsymbol{H} \to \boldsymbol{H}_0 + \boldsymbol{H}_1. \tag{5}$$

Retaining terms of only first order and combining this with the expression for the PLDoS, we obtain the following expression giving the update to the position of the n^{th} scatterer for iteration i

$$\boldsymbol{r}_n^{i+1} = \boldsymbol{r}_n^i + \Delta\boldsymbol{r}_n \times \mathrm{sign}\Big[\mathrm{Im}\Big\{\xi^2\overleftrightarrow{\boldsymbol{G}}(\boldsymbol{r},\boldsymbol{r}_n)\cdot\overleftrightarrow{\boldsymbol{\alpha}}_E\cdot\nabla\boldsymbol{E}_0(\boldsymbol{r}_n) + i\xi\overleftrightarrow{\boldsymbol{G}}_{EH}(\boldsymbol{r},\boldsymbol{r}_n)\cdot\overleftrightarrow{\boldsymbol{\alpha}}_H\cdot\nabla\boldsymbol{H}_0(\boldsymbol{r}_n)\Big\}\Big]. \tag{6}$$

where $\Delta\boldsymbol{r}_n$ is the size of the step. Choosing to update the position in this way is guaranteed to lead to an increase in the PLDoS.

3 Numerical Examples

We aim to design a metasurcace which manipulates antenna radiation in a particular way. To do so, we present several numerical examples of the semi-analytic optimization procedure we have derived. While our results are completely general, we choose the parameters at optical wavelengths for our numerical examples: wavelength $\lambda = 550$ nm and scatterer radius $r_0 = 65$ nm. First, we apply our method to increase the power emission of an electric dipole emitter. The results of this are shown in Figure 1. We choose, arbitrarily, an initial structure shown in Figure 1(a), and apply our iterative optimization procedure to design the structure shown in Figure 1(c), yielding a three-fold enhancement in the power emission of the dipole emitter. Furthermore, by examining the eigenmodes and eigenvectors of the interaction matrix (3), the mechanism for this enhancement can be explained. Figure 1(d) shown the dominant eigenmode in the initial configuration and Figure 1(f) shown the dominant eigenmode in the final configuration. The eigenvalue of the dominant mode has increased by a factor of ~ 3, which can be interpreted as an enhancement of the collective response of the system. Additionally, the spatial distribution of the mode has changed to increase the overlap with the dipole emitter.

Next, we apply our method to engineer the far-field radiation pattern of a dipole emitter, shown in Figure 2. Starting from the structure shown in Figure 2(a), our optimization procedure is applied to enhance the power emitted along the $x \to \infty$ direction. The resulting structure is shown in Figure 2(b) and the change in radiation pattern is shown in Figure 2(c). It is clear from these plots that the structure we have designed exhibits clear beaming along the desired direction.

As a final interesting example, we show that more complex functionality can be obtained from structures designed using the method presented here by multiplexing the designed structures. For example, the functionality of a Luneburg

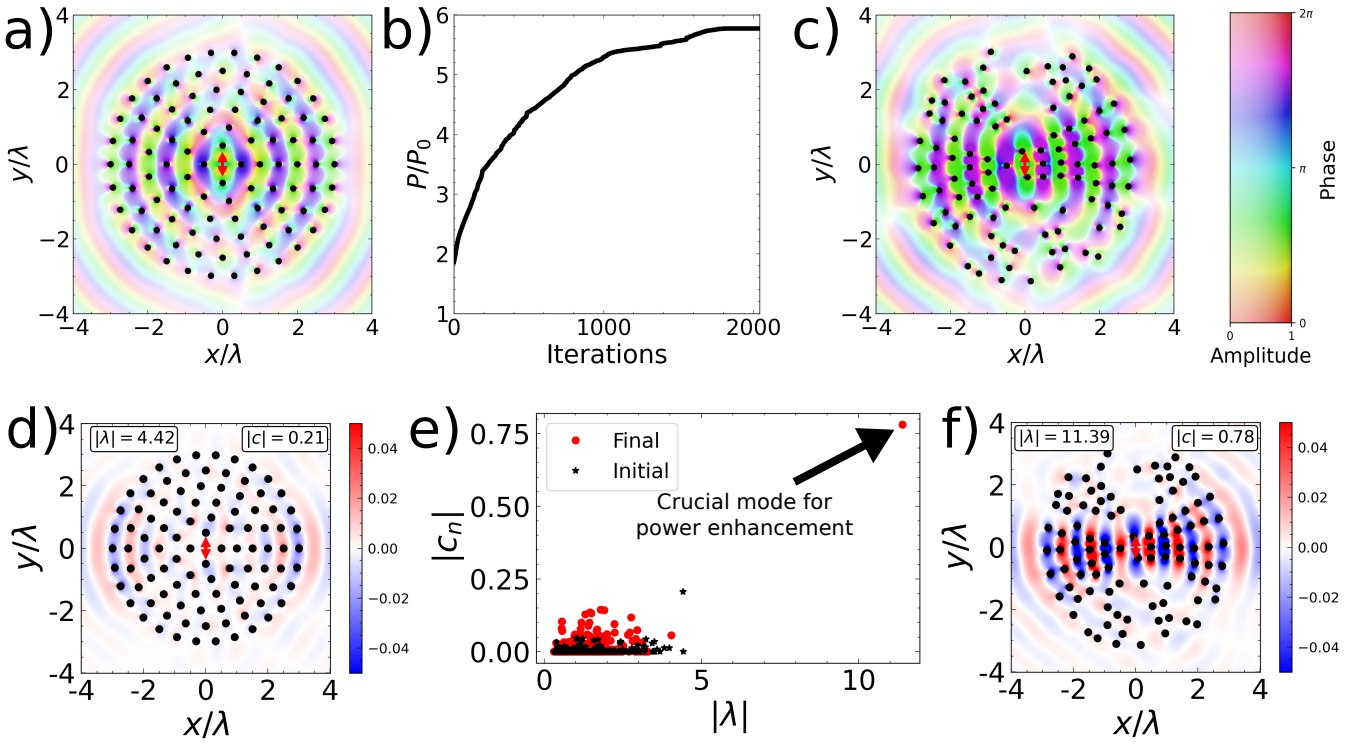

Figure 1. The result of applying our design methodology to enhance power emission of a dipole using 100 scatterers. In all plots, scatterers are shown as black circles and the dipole emitter as a red arrow. (a) Shows the $\hat{\boldsymbol{y}}$ component of the electric field in the initial configuration, (b) shows the progress of the power enhancement as the optimisation progresses and (c) shows $\mathrm{Re}[\boldsymbol{E}\cdot\hat{\boldsymbol{y}}]$ in the optimised configuration. (d) and (f) show $\mathrm{Re}[\boldsymbol{E}\cdot\hat{\boldsymbol{y}}]$ of the mode with the largest expansion coefficient in the initial and optimised structure respectively. (e) shows how the eigenvalues and expansion coefficients change due to the optimisation. The final mode, plotted in (f), with eigenvalue ~ 12 is responsible for the power enhancement.

lens is shown in Figure 3(a). For a certain choice of radially graded index profile, a point source placed upon the exterior of the lens is converted into a plane wave. Due to the angular symmetry of the profile, rotating the point souce allows the plane wave to be steered. This behaviour can be roughly approximated by multiplexing the structure shown in Figure 2(c). We demonstrate this in Figure 3(b,c). Rotating the source through the multiplexed structure allows for the re-direction of emitted radiation with manageable back-lobes. Rather than continuous control, the approximate Luneburg lens gives only discrete angular resolution. For larger angular resolution, the size of the device must be increased.

4 Conclusions & Outlook

In this work, we have derived a method of designing metamaterials comprised of small scatterers. This has been applied to design aperiodic planar structures that have a predetermined effect on both the near and the far–field of a dipole emitter. In the near-field, power emission has been enhanced by a factor of ~ 3 and the far-field radiation pattern has been made highly directional. We have also demonstrated that structures designed in this way may be multiplexed to achieve more complex functionality. As an example, we approximate the functionality of a Luneburg lens using an array of dipole scatterers.

As well as an iterative design methodology, we propose an interesting physical interpretation of the eigenvalues and eigenvectors of the matrix defining the electromagnetic response of the scattering system. The eigenvalues of the system correspond to eigen-polarizabilities which we attribute to several scatterers responding collectively. A large collective response corresponds to a large eigenvalue. By analysing how the eigenvalues and eigenvectors change over the optimisation procedure, we have identified that power emission is enhanced by a large collective response of the scatterers, corresponding to a large eigenvalue while directivity is achieved by modifying the spatial distribution of the modes, without significant change to the eigenvalues.

The applicability of both our design technique and theoretical understanding are not limited to engineering dipole radiation. A perturbative approach to designing electromagetic field properties might be applied to engineering mode distributions in optical fibers or metalenses. If more arbitrary field distributions could be successfully designed, then this method might find utility in constructing metasurface holograms or to perform wavefront shaping when imaging through disordered media. As our approach automatically takes non-locality into account, it may be also

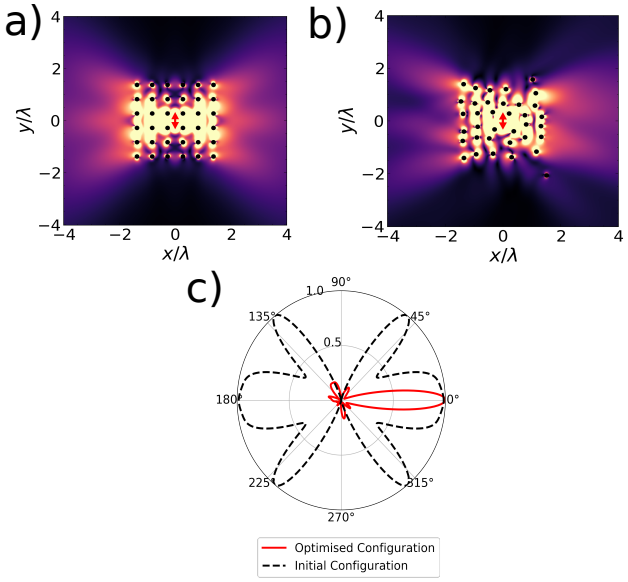

Figure 2. Re-structuring far-field of a dipole emitter to be directed along $\theta = 0°$, using 36 scatterers. (a) shows $|\boldsymbol{E}|$ for the initial configuration, where scatterers are black circles and the emitter is shown as a red arrow. (b) shows $|\boldsymbol{E}|$ in the optimized structure. (c) shows a comparison of the far-field distribution of the Poynting vector for the initial configuration (black dashed line) and the optimised configuration (red line). The width of the beam in the optimised structure is $\sim 24°$.

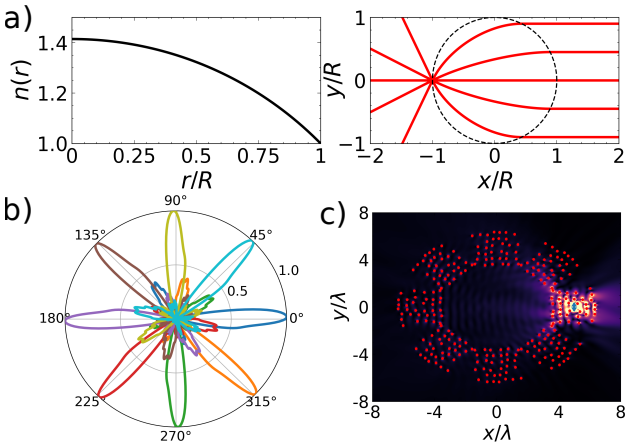

Figure 3. Multiplexing the design shown in Figure 2 to construct a scattering structure approximating the functionality of a Luneburg lens. (a) demonstrates the function of a normal Luneburg lens of radius R, with a refractive index graded according to the inset equation. A point source is converted into a beam in a single direction. (b) and (c) The result of multiplexing the structure proposed in Figure 2 to produce a Luneburg lens with a discrete angular resolution of 45°. By rotating the source and changing it's location inside the array the far-field Poynting vectors indicated in (b) can be observed.

used to develop and provide insight into non-local metasurfaces.

Acknowledgements

We acknowledge financial support from the Engineering and Physical Sciences Research Council (EPSRC) of the United Kingdom, via the EPSRC Centre for Doctoral Training in Metamaterials (Grant No. EP/L015331/1). J.R.C also wishes to acknowledge financial support from Defence Science Technology Laboratory (DSTL). S.A.R.H acknowledges financial support from the Royal Society (RPG-2016-186).

References

1. Quevedo-Teruel, O. *et al.* Roadmap on metasurfaces. *Journal of Optics* **21,** 073002 (2019).
2. Mosk, A. P., Lagendijk, A., Lerosey, G. & Fink, M. Controlling waves in space and time for imaging and focusing in complex media. *Nature Photonics* **6,** 283–292 (2012).
3. Ma, G. & Sheng, P. Acoustic metamaterials: From local resonances to broad horizons. *Science Advances* **2,** e1501595 (2016).
4. Chen, H.-T., Taylor, A. J. & Yu, N. A review of metasurfaces: physics and applications. *Reports on Progress in Physics* **79,** 076401 (2016).
5. Chen, W. T., Zhu, A. Y. & Capasso, F. Flat optics with dispersion-engineered metasurfaces. *Nature Reviews Materials* (2020).
6. Faenzi, M. *et al.* Metasurface Antennas: New Models, Applications and Realizations. *Scientific Reports* **9,** 1–14 (2019).
7. Ni, X., Kildishev, A. V. & Shalaev, V. M. Metasurface holograms for visible light. *Nature Communications* **4** (2013).
8. Jang, M. *et al.* Wavefront shaping with disorder-engineered metasurfaces. *Nature Photonics* **12,** 84–90 (2018).
9. Díaz-Rubio, A., Li, J., Shen, C., Cummer, S. A. & Tretyakov, S. A. Power flow–conformal metamirrors for engineering wave reflections. *Science Advvances* **5,** eaau7288 (2019).
10. Molesky, S. *et al.* Inverse design in nanophotonics. *Nature Photonics* **12,** 659–670 (2018).
11. Xu, L. *et al.* Enhanced Light-Matter Interactions in Dielectric Nanostructures via Machine Learning Approach. *Advanced Photonics* **2,** 026003 (2020).
12. Wiecha, P. R., Arbouet, A., Cuche, A., Paillard, V. & Girard, C. Decay rate of magnetic dipoles near non-magnetic nanostructures. *Physical Review B* **97,** 1–7 (2018).